International Journal of Heat and Mass Transfer 172 (2021) 121161

Contents lists available at ScienceDirect

International Journal of Heat and Mass Transfer

journal homepage: www.elsevier.com/locate/hmt

From lab and up: superior and economic heat transfer performance of ionanofluids containing long carbon nanotubes and 1-ethyl-3-methylimidazolium thiocyanate

Bertrand Jóźwiak[a], Grzegorz Dzido[b], Anna Kolanowska[a], Rafał G. Jędrysiak[a], Edward Zorębski[c], Heather F. Greer[d], Marzena Dzida[c,*], Sławomir Boncel[a,*]

[a] Silesian University of Technology, Faculty of Chemistry, Department of Organic Chemistry, Bioorganic Chemistry and Biotechnology, Bolesława Krzywoustego 4, 44-100 Gliwice, Poland
[b] Silesian University of Technology, Faculty of Chemistry, Department of Chemical Engineering and Process Design, Marcina Strzody 7, 44-100, Gliwice, Poland
[c] University of Silesia in Katowice, Institute of Chemistry, Szkolna 9, 40-006 Katowice, Poland
[d] University of Cambridge, Yusuf Hamied Department of Chemistry, Lensfield Road, Cambridge, CB2 1EW, UK

ARTICLE INFO

Article history:
Received 11 January 2021
Revised 22 February 2021
Accepted 24 February 2021

Keywords:
Ionanofluid laminar flow
Heat transfer efficiency
Convective heat transfer coefficient
Pressure drop
Performance evaluation criterion
Efficiency-price index

ABSTRACT

The optimization of energy systems and the efficiency enhancement of energy conversion processes are still huge challenges. The ionanofluids (INFs) composed of the long multi-walled carbon nanotubes (MWCNTs) and 1-ethyl-3-methylimidazolium thiocyanate ionic liquid ([C_2C_1im][SCN]) are innovative systems with proven remarkably enhanced thermal conductivity and attractive rheological characteristics. Therefore, as an extension of our previous study, this work aims to examine the overall heat transfer performance of these INFs as working fluids for energy conversion processes and design sustainable energy systems. The new measuring set was designed and constructed to determine the convective heat transfer coefficient and pressure drop during the flow of INFs, using the heat exchanger with saturated steam at 100°C. The obtained results showed that the heat transfer of INFs is prevailed by the convection mechanism. According to a new thermo-economic efficiency-price index proposed in this work, the amalgamation of MWCNTs with [C_2C_1im][SCN] is justified from both thermophysical and economic points of view.

1. Introduction

Energy is considered a major agent in the generation of wealth and economic development [1]. Nonetheless, global environmental issues significantly affect patterns of energy use around the world. It is, therefore, necessary to optimize energy balance which enables more efficient thermal systems in many industries, such as microelectronics, automobiles, power generation, and many others. Of particular interest are the applications related to *i*) photovoltaic/thermal solar systems, *ii*) heat pump systems, *iii*) engine cooling or vehicle thermal management, and *iv*) heating, ventilation, and air conditioning [1–9]. Lots of modern thermal systems involve the combined heat and mass transfer phenomena, which result in the need for comprehensive exergy analysis [4–7]. Importantly, the optimum operation of any thermal system requires minimum energy destruction [4].

One of the top strategies to enhance the thermal performance of heat transfer fluids (HTFs) for storage, transportation, and conversion of energy in modern thermal systems is the addition of nanometer-sized, thermally-conductive (polymeric, metallic, organic, or inorganic) solid particles of various morphological properties into a base liquid (water, oil, ethylene glycol, etc.) [10]. Multi-walled carbon nanotubes (MWCNTs) are particularly useful for this purpose due to both low density of ca. 2 $g \cdot cm^{-3}$ and very high thermal conductivity up to 3000 $W \cdot m^{-1} \cdot K^{-1}$ at room temperature [11]. The nanofluids (NFs) have been extensively examined as working media in solar collectors including both thermal and thermo-economic aspects [12–14].

A new type of heat transfer media, so-called ionanofluids (INFs), has been intensively studied in recent years. This is a group of nanodispersions in which ionic liquids (ILs) form the continuous phase [15]. ILs have many advantages over molecu-

* Corresponding authors
E-mail addresses: marzena.dzida@us.edu.pl (M. Dzida), slawomir.boncel@polsl.pl (S. Boncel).

https://doi.org/10.1016/j.ijheatmasstransfer.2021.121161

Nomenclature

Acronyms and abbreviations

$[C_1C_1im][DMP]$	1,3-dimethylimidazolium dimethylphosphate
$[C_2C_1im][DCA]$	1-ethyl-3-methylimidazolium dicyanamide
$[C_2C_1im][EtSO_4]$	1-ethyl-3-methylimidazolium ethylsulfate
$[C_2C_1im][MeSO_3]$	1-ethyl-3-methylimidazolium methanesulfonate
$[C_2C_1im][SCN]$	1-ethyl-3-methylimidazolium thiocyanate
$[C_2C_1im][TCM]$	1-ethyl-3-methylimidazolium tricyanomethanide
$[C_4C_1im][NTf_2]$	1-butyl-3-methylimidazolium bis(trifluoromethylsulfonyl)imide
$[C_4C_1pyrr][NTf_2]$	1-butyl-1-methylpyrrolidinium bis(trifluoromethylsulfonyl)imide
$[C_6C_1im][BF_4]$	1-hexyl-3-methylimidazolium tetrafluoroborate
c-CVD	catalytic chemical vapor deposition
GNPs	graphene nanoplatelets
GO	graphene oxide
HTA	heat transfer area
HTF	heat transfer fluid
IL	ionic liquid
INF	ionanofluid
MWCNT	multi-walled carbon nanotube
NF	nanofluid

Parameters and variables

C_p	specific isobaric heat capacity of fluid ($J \cdot kg^{-1} \cdot K^{-1}$)
d	inner diameter of measuring tube (m)
d_o	outer diameter of measuring tube (m)
EPI	efficiency-price index (–)
f	Darcy friction factor (–)
g	acceleration of gravity ($m \cdot s^{-2}$)
G	mass flow rate of fluid ($kg \cdot s^{-1}$)
h	average convective heat transfer coefficient ($W \cdot m^{-2} \cdot K^{-1}$)
k	thermal conductivity of fluid ($W \cdot m^{-1} \cdot K^{-1}$)
L	length of measuring tube (m)
Nu	average Nusselt number (–)
Pe	Peclet number (–)
PEC	performance evaluation criterion (–)
Pr	Prandtl number (–)
Re	Reynolds number (–)
T	average bulk temperature of fluid (°C)
T_{in}	inlet bulk temperature of fluid (°C)
T_{out}	outlet bulk temperature of fluid (°C)
T_w	average wall temperature of measuring tube (°C)
v	average velocity of fluid ($m \cdot s^{-1}$)
Δh_m	difference in height of mercury in manometer limbs (m)
Δp	pressure drop (Pa)
ΔT_{LMTD}	logarithmic mean temperature difference (°C)
η	viscosity of fluid (Pa·s)
η_w	viscosity of fluid at average wall temperature (Pa·s)
ρ	density of fluid ($kg \cdot m^{-3}$)
ρ_m	density of mercury ($kg \cdot m^{-3}$)
$\$_{INF}$	total cost of INF preparation ($)
$\$_{IL}$	price of base IL ($)
$\$_{MWCNTs}$	total cost of MWCNT synthesis ($)
$\$_{UT}$	cost of ultrasound treatment ($)

Subscripts

exp	experimental
pred	predicted
1,2,3,4,5	thermocouple numbering on the wall of measuring tube

lar base fluids: high chemical and thermal stabilities, wide liquidity range, negligible vapor pressure, designable cation-anion structure, low flammability, and acceptable recyclability [16,17]. The INFs have rapidly gained many possibilities for application, such as working fluids for energy transport in cooling and heating systems (solar collectors, heat pumps, etc.) [18–22], pigments in paints for solar panels [23], electrolytes in cell batteries [24], or lubrication materials [25,26]. In areas related to thermal management and energy harvesting, the thermophysical properties of INFs (thermal conductivity, viscosity, isobaric heat capacity, density) play a key role [27–30]. They are crucial in determining the heat transfer (or storage) capabilities and the required pumping power.

The most promising thermophysical properties have cyano alkylimidazolium-based INFs due to relatively high thermal conductivity and low viscosity of their base liquids compared to other known ILs [31]. Recently, we found an extraordinary 43.1% improvement of thermal conductivity of INF containing 1-ethyl-3-methylimidazolium thiocyanate $[C_2C_1im][SCN]$ and 1 wt% in-house 7h MWCNTs with a high aspect ratio of 6300 ("7h" refers to the duration of the catalytic chemical vapor deposition (c-CVD)), while the nanodispersion viscosity remained at a moderate level of 135 mPa·s (25°C, shear rate of 32 s^{-1}) [32]. Lower MWCNTs loading of 0.25 wt% enhanced the thermal conductivity of INF by 9.6% and increased its viscosity from 23.6 mPa·s to 46.0 mPa·s under the same conditions as above. Furthermore, we discovered that the thermal conductivity of the interfacial nanolayer is 39 times higher than that of the base $[C_2C_1im][SCN]$.

In contrast to thermophysical investigations of INFs, only very few experimental studies concern the heat transfer performance of this type of media. Paul et al. [22,33,34] investigated the natural and forced convection of INFs containing 0.18 vol%, 0.36 vol%, 0.9 vol%, as well as 0.5 wt%, 1.0 wt%, and 2.5 wt% of alumina oxide Al_2O_3 nanoparticles (spherical and whiskers shape, size $<$ 50 nm, specific surface area $>$ 40 $m^2 \cdot g^{-1}$) dispersed in 1-butyl-3-methylimidazolium bis(trifluoromethylsulfonyl)imide $[C_4C_1im][NTf_2]$ or 1-butyl-1-methylpyrrolidinium bis(trifluoromethylsulfonyl)imide $[C_4C_1pyrr][NTf_2]$, respectively. The results indicate that during forced convection the heat transfer coefficient increases with nanoparticle loading up to 27% and 40% for laminar and turbulent flow regimes, respectively [22]. On the other hand, the reverse trend is observed for natural convection. In this case, the decrease in convective heat transfer coefficient with Al_2O_3 concentration occurs regardless of the nanoparticle morphological characteristics and aspect ratio of the rectangular test cell [34]. This result derives from several overlapping factors associated with a relative change in the thermophysical properties of INFs, nanoparticle clustering, and nanoparticle-IL interactions.

Numerical analyses of the heat transfer performance of INFs [19,21,35–41] are much more common than the above-mentioned experimental works. Minea and Murshed [35] reported that low concentrations ($\leq$ 1 wt%) of graphene nanoplatelets (GNPs) or MWCNTs (with an aspect ratio of ca. 70–700) in $[C_4C_1im][NTf_2]$, 1-hexyl-3-methylimidazolium tetrafluoroborate $[C_6C_1im][BF_4]$, or 1-ethyl-3-methylimidazolium ethylsulfate $[C_2C_1im][EtSO_4]$ resulted in moderate enhancement of heat transfer coefficient, between 1.7% and 12.1% over the base ILs, during forced convection in laminar flow regime. Chereches et al. [41] conducted a simulation of

heat transfer during laminar flow of mixtures containing water (0, 0.25, 0.5, or 0.75 mole fraction), 1-ethyl-3-methylimidazolium methanesulfonate $[C_2C_1im][MeSO_3]$, and several loadings (1 wt%, 2.5 wt%, 5 wt%, 10 wt%, or 15 wt%) of Al_2O_3 nanoparticles (size < 50 nm, specific surface area > 40 $m^2 \cdot g^{-1}$). They concluded that the addition of water to IL decreases the convective heat transfer coefficient up to 70%, while the addition of nanoparticles enhances the heat transfer by a maximum of 50%, depending on the alumina loading. Prasad and Selvakumar [21] studied laminar forced convection in a heated rectangular tube (geometry commonly used in flat plate solar collectors) using INFs consisted of $[C_4C_1im][NTf_2]$ and Al_2O_3 nanoparticles (size < 50 nm, specific surface area > 40 $m^2 \cdot g^{-1}$) up to 2.5 wt%. They noted that the heat transfer performance of the INFs increased with Reynolds number, nanoparticle concentration, and temperature. The maximum enhancement of the convective heat transfer coefficient reached ca. 60% and 40% compared to base IL and reference water-based NF, respectively. The research indicates that INFs have a higher potential to be employed in medium to high temperature applications. Similar conclusions were reached by Hosseinghorbani et al. [19] who investigated forced convection in the turbulent flow regime of INFs composed of graphene oxide (GO) nanoparticles (0.5 wt%, 1 wt%, or 2 wt%) and $[C_4C_1im][NTf_2]$. They noted that the maximum enhancement in convective heat transfer coefficient of INFs (compared to base IL) was equal to 7.2% at 0.5 wt% loading of GO. Higher nanoparticle concentrations cause a significant increase in the viscosity of INFs, which surpasses the positive enhancement of other physicochemical properties, especially thermal conductivity. The work of Hosseinghorbani et al. [19] demonstrates that INFs at low mass fractions of GO are superior to the commercial HTFs, and have great potential for use in concentrated solar power plants. Recently, Das et al. [8] numerically examined the performance of hybrid photovoltaic/thermal solar system with INFs composed of 1,3-dimethylimidazolium dimethylphosphate $[C_1C_1im][DMP]$ (20 vol%), water (80 vol%), and two-dimensional MXene Ti_3C_2 nanosheets (0.05 wt%, 0.10 wt%, or 0.20 wt%). The convective heat transfer coefficient increases by 12.6% for 0.20 wt% Ti_3C_2 + $[C_1C_1im][DMP]$/water INF compared to the reference Al_2O_3/water NF at a mass flow rate of 0.06 $kg \cdot s^{-1}$.

Alirezaie et al. [42,43], who made interesting thermo-economic analyzes of conventional water and ethylene glycol-based NFs using various engineering correlations available in the literature, concluded that "nanofluids don't have economic justification except in high-tech devices with critical applications". However, they did not take into account the possibility of using the INFs. The influence of thermophysical properties and economic costs of ILs and INFs on their feasibility as HTFs in chemical process design has been extensively studied by Nieto de Castro group [28,44,45]. França et al. [45] reported that an efficient way to study new design expenses is to divide them into five parts, i.e., the battery limits, utility, off-site, engineering fees, and working capital. The main influence herein is the battery limits investment, which is related to the equipment and installation costs. This is a function of the device size (heat transfer area (HTA)), construction material, and assumed working conditions (pressure, temperature). Mendonça et al. [44] considered an exemplary application of heat exchanger and condenser, prescribing the external constraints and neglecting the pressure drop across the fluid ducts. Consequently, the number of relevant variables has been reduced to HTA expressed by Newton's law of cooling. The conclusion was that without the correct physicochemical properties of the working medium, it was possible to overestimate the required equipment size by 25%, which can significantly increase the economic costs of the process. França et al. [28] selected a specific process and calculated the necessary HTA considering the use of ILs, INFs, and commercial HTFs. They found that $[C_2C_1im]^+$-based and cyano-based INFs yield smaller HTA due to their lower viscosity. Therefore, these media are efficient on a par with a significant number of commercial HTFs. The addition of MWCNTs to the ILs leads to an increase in the required equipment size, however, at moderate nanoparticle doses of ca. 0.5 wt%, it improves the thermophysical properties and reduces the variation of the HTA with temperature. Although the high price of ILs represents an obstacle, some of the ILs and INFs require a smaller HTA than the commercial HTFs for the same purpose, especially at temperatures above 80°C [28]. Oster et al. [30] analyzed thermophysical characteristics and economic aspects of heat exchange reactor at 25°C and 90°C for trihexyl(tetradecyl)phosphonium-based ILs with acetate, butanoate, hexanoate, octanoate, or decanoate anions, as well as for INFs composed of above-mentioned ILs and MWCNTs (with an aspect ratio of ca. 100), boron nitride, graphite, or mesoporous carbon, with concentration up to 3 wt%. Their studies showed that the INFs do not seem to be promising materials for heat transfer applications. Despite the enhanced thermal conductivity, density, and isobaric heat capacity (which are beneficial), the viscosity is also augmented, thereby significantly increasing maintenance costs of the equipment. They pointed pristine ILs as promising HTFs, particularly at high temperatures due to the decrease in viscosity, low vapor pressure, and wide liquidity range [30].

Taking into account all the above-mentioned studies and our previous investigations, the research objectives of this work include three main areas that have not been presented in the literature so far: *i*) fully experimental study of the heat transfer of INFs containing long MWCNTs during forced convection in laminar flow regime (currently there are only numerical works); *ii*) in-depth analysis of the "negative effects" of heat transfer during the flow of INFs, i.e., the pressure drop penalty (it is often neglected in the literature); *iii*) proposal of a simple parameter/indicator that does not require an exergy balance, but clearly shows the cost-effectiveness of using INFs in heat transport applications (currently the costs of added nanoparticles and INF preparation are not included).

In particular, this work is focused on the overall heat transfer performance of low-viscosity cyano alkylimidazolium-based INFs containing $[C_2C_1im][SCN]$ and 0.100 wt%, 0.175 wt%, or 0.250 wt% loadings of in-house 7h MWCNTs with a high aspect ratio equal to 6300. The research helps to deeper understand the behavior of INFs during forced convection in the laminar flow regime through the straight horizontal tube, i.e., the case commonly found in heat exchange applications. It is essential to evaluate the overall energy efficiency of a thermal system since the enhancement in convective heat transfer coefficient may be negated by the increase in pressure drop and the required pumping power. To the best of our knowledge, the pressure drop penalty during the flow of INFs has not yet been investigated experimentally. Therefore, we designed and constructed a new experimental stand to determine the heat transfer performance of INFs. The major advantages of the proposed set are the measurement capabilities of convective heat transfer coefficient and pressure drop of low-volume nanofluid samples (up to 150 mL), as well as the ability to study possible applications of a steam heat exchanger for energy transport using IL and INFs as working fluids. Finally, we proposed a new non-dimensional thermo-economic efficiency-price index to examine the justification of the amalgamation of MWCNTs with IL.

2. Materials and methods

2.1. Materials

The continuous phase of studied INFs was commercial $[C_2C_1im][SCN]$ (CAS Number: 331717-63-6, Sigma Aldrich, USA).

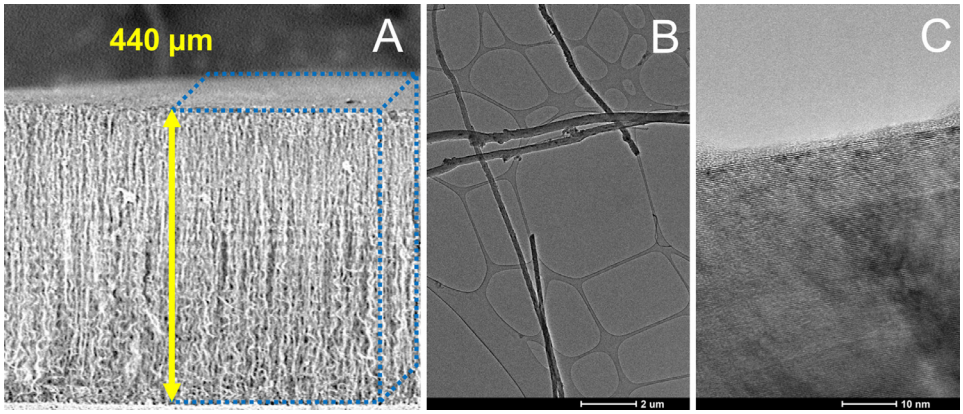

Fig. 1. Representative SEM image of vertically aligned MWCNT array **(A)** and TEM images of low **(B)** and high **(C)** magnification of individual MWCNTs.

The advantages of the chosen IL are high thermal conductivity along with low viscosity and ecotoxicity in comparison to other known ILs [28,31,32]. The dispersed phase of INFs consisted of MWCNTs, which were synthesized in our laboratory via seven-hour c-CVD, according to the methodology described in ref. [46]. We have used the same batch of materials, thus, the detailed specification of $[C_2C_1im][SCN]$ and in-house 7h MWCNTs can be found in our previous work [32]. Briefly recalling, Fig. 1 shows micro and nanomorphology of applied MWCNTs.

Scanning electron microscopy (SEM) image (Fig. 1A) revealed as-grown MWCNTs as vertically aligned arrays 440 μm-thick (which practically correspond to the actual length of a single nanotube), partially curly at the side of growth. Further, transmission electron microscopy (TEM) images at low (Fig. 1B) and high (Fig. 1C) magnification show individual nanotubes (diameter ca. 60–80 nm, aspect ratio 6300, BET surface 35 $m^2 \cdot g^{-1}$) as straight *quasi*-1D objects with a scarce number of corrugations and of a particularly high graphitization degree at the whole cross-section – apart from a very few near-surface walls richer in C-sp^3-defects (less developed upon the final step of c-CVD growth). A Thermo Scientific (FEI) Talos F200X G2 operating at 200kV was utilized for TEM analysis. TEM images were acquired using a Ceta 4k × 4k CMOS camera. The MWCNTs were dispersed on a copper grid (300 mesh) with holey carbon film.

2.2. Sample preparation

The INFs were prepared by dispersing 0.100 wt%, 0.175 wt%, and 0.250 wt% (i.e., 0.0531 vol%, 0.0930 vol%, and 0.133 vol%) of in-house 7h MWCNTs in 150 mL of $[C_2C_1im][SCN]$. The samples were sonicated for 10 min using UP200St sonicator (Hielscher Ultrasonics GmbH, Germany). The ultrasound generator of the device operated at its nominal values of power, frequency, and amplitude (200 W, 26 kHz, and 100%, respectively). To prevent the increase in temperature during sonication, the samples were placed in a 1000 mL beaker with cooled (−5°C) pure ethylene glycol (POCH, Poland). The nanodispersions under test were stable during the experiments, however, over a longer time scale of more than six months, they tended to sediment. Details on the stability of the tested INFs can be found in our previous work [32].

2.3. Measurement of thermophysical properties

The specific isobaric heat capacity of pristine $[C_2C_1im][SCN]$ and INF with 1 wt% loading of in-house 7h MWCNTs was measured using a differential temperature-scanning microcalorimeter (DSC) and batch type measurement cells (made of Hastelloy) in a temperature range of 25°C–50°C. The expanded uncertainty (coverage factor 2.0, confidence level 0.95) of specific isobaric heat capacity measurements was estimated to be ±2%. Details about apparatus, calibration, and measurement procedures can be found in ref. [32]. The thermal conductivity of pure $[C_2C_1im][SCN]$ and INFs containing 0.100 wt% and 0.250 wt% of in-house 7h MWCNTs was measured in a temperature range of 25°C–50°C. Thermal conductivity was measured using KD2 Pro Thermal Properties Analyzer (Decagon Devices Inc., Pullman, USA) with a single needle KS-1 sensor of 1.3 mm diameter and 60 mm length; the estimated uncertainty was ±5%. The measurements were performed according to the procedure described in detail in our previous work [32].

2.4. Measurement of heat transfer performance

The heat transfer performance of INFs was investigated using a new custom-designed experimental set for low-volume samples up to 150 mL, shown schematically in Fig. 2. The main section of the test stand was a steam heat exchanger (1). In its lower part, there was an electric heater (2) immersed in distilled water. Its heating power was controlled by an autotransformer (3) VT5-1 (PowerLab, Malaysia) with aconstant voltage setting of 130 V. The tank (1) was thermally insulated with glass wool and had a small opening with a condenser (4), which ensured that the produced steam remained at atmospheric pressure. The saturated steam of 100°C heated a cylindrical horizontal measuring tube (5) made of stainless steel AISI 316L (inner diameter d = 1.53 mm, outer diameter d_o = 2.01 mm, and length L = 280 mm), through which the studied fluid was pumped using a non-pulsating syringe pump (6) NE-1010 (New Era Pump Systems, USA). The flow was laminar and fully-developed, i.e., undisturbed by the entrance and exit effects due to the proper measuring tube geometry $L/d >> 50$. The exact fluid flow rate was determined using a laboratory balance (7) PS 1200/C/2 (Radwag, Poland) of 0.01 g precision and a digital stopwatch, by defining the time required to collect a certain mass of the sample in a sealed bottle. Besides, seven K-type thermocouples with a standard uncertainty of ±0.1°C were mounted along the measuring tube (5), two inside at its inlet and outlet, and five on the outer wall at equal intervals, to measure bulk fluid temperature and local wall temperatures, respectively. The real-time temperature measurement and archiving of the results were enabled by the data acquisition module (8) USB-4718 (Advantech, Taiwan) connected to a computer with a graphical user interface (9). Furthermore, a U-tube mercury manometer (10) was used for the determination of pressure drop across the test section with an accuracy of 1 mm Hg. After each measurement, a sealed sample was cooled to the ambient temperature in the laboratory and then used for further experiments at increasingly higher flow rates within the

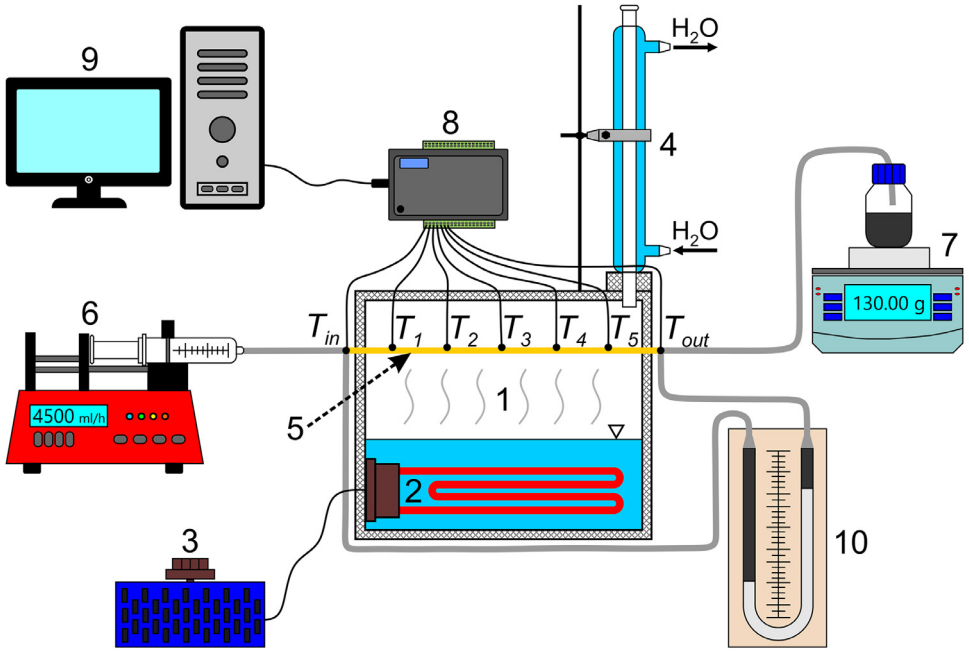

Fig. 2. Diagram of the custom-designed experimental set for the investigation of heat transfer performance of INFs: (1) steam heat exchanger, (2) electric heater, (3) autotransformer, (4) condenser, (5) measuring tube, (6) syringe pump, (7) laboratory balance, (8) data acquisition module, (9) computer with a graphical user interface, (10) U-tube mercury manometer.

range of ca. 100–4500 mL·h^{-1} with the step of 100 mL·h^{-1} or 200 mL·h^{-1}. All the measurements were carried out in single series without repetitions.

The average bulk temperature T of the analyzed fluid was determined as the arithmetic mean between temperatures at inlet T_{in} and outlet T_{out} of the measuring tube (see Fig. 2):

$$T = \frac{T_{in} + T_{out}}{2}. \quad (1)$$

The average wall temperature T_w of the measuring tube was calculated as the arithmetic mean from the indications of thermocouples T_1–T_5 (see Fig. 2):

$$T_w = \frac{T_1 + T_2 + T_3 + T_4 + T_5}{5}. \quad (2)$$

The values of T and T_w varied from 64.1°C to 38.3°C and from 99.2°C to 97.2°C, respectively, depending on the mass flow rate of analyzed fluid G ($2.31 \cdot 10^{-5}$–$1.42 \cdot 10^{-3}$ kg·s^{-1}).

The experimental values of the average convective heat transfer coefficient h were obtained from the heat balance [47,48]:

$$h = \frac{GC_p(T_{out} - T_{in})}{\pi dL \cdot \Delta T_{LMTD}} \quad (3)$$

where C_p is the specific isobaric heat capacity of fluid at T (Table S1 in Supplementary Material and Table S5 in Supplementary Material of our previous work [32]); d and L are the internal diameter and length of measuring tube, respectively; and ΔT_{LMTD} is the logarithmic mean temperature difference, describing the temperature driving force for heat transfer in flow system (heat exchanger), defined as [49]:

$$\Delta T_{LMTD} = \frac{(T_w - T_{in}) - (T_w - T_{out})}{\ln\left(\frac{T_w - T_{in}}{T_w - T_{out}}\right)}. \quad (4)$$

ΔT_{LMTD} ranged from 20.2°C to 58.0°C depending on the fluid flow rate ($2.31 \cdot 10^{-5}$–$1.42 \cdot 10^{-3}$ kg·s^{-1}).

Furthermore, the experimental values of the pressure drop Δp during the flow of analyzed fluid were determined from the formula [50]:

$$\Delta p = \Delta h_m(\rho_m - \rho)g \quad (5)$$

where Δh_m is the difference in height of mercury in the manometer limbs, ρ_m is the density of mercury (13550 kg·m^{-3} at 20°C), ρ is the density of tested fluid at T (Table S2 in Supplementary Material and Table S6 in Supplementary Material of our previous work [32]), and g is the acceleration of gravity.

The measurement uncertainties of average convective heat transfer coefficient h and pressure drop Δp were estimated based on the error propagation law using the method presented by Moffat [51]. The calculated relative combined standard uncertainties are equal to ±6% and ±11% for h and Δp, respectively. A detailed uncertainty analysis is provided in Part III of the Supplementary Material.

2.4.1. Experimental validation

The experimental stand was validated by measuring the average convective heat transfer coefficient and pressure drop for pristine [C_2C_1im][SCN], which is a Newtonian liquid, and whose physicochemical properties (thermal conductivity, specific isobaric heat capacity, density, viscosity) have been investigated in this work (Tables S1–S3 in Supplementary Material), as well as in our previous study [32] (Tables S4–S7 and Fig. S3 in Supplementary Material of ref. [32]). The measurements were conducted within the flow rate range of 100–4500 mL·h^{-1} with the step of 100 mL·h^{-1} or 200 mL·h^{-1}.

The obtained experimental results of the convective heat transfer coefficient for [C_2C_1im][SCN] were compared with the values calculated from the Sieder-Tate equation for laminar flow heat transfer in a circular tube and constant wall temperature boundary condition [52,53], which strictly corresponded to our measurement case:

$$h = 1.86\frac{k}{d}\left[RePr\frac{d}{L}\right]^{\frac{1}{3}}\left(\frac{\eta}{\eta_w}\right)^{0.14} \quad (6)$$

with the following constraints [52,53]:

$$13 \le Re \le 2030\ ,\ 0.48 \le Pr \le 16700\ ,\ 0.0044 \le \frac{\eta}{\eta_w} \le 9.75 \quad (7)$$

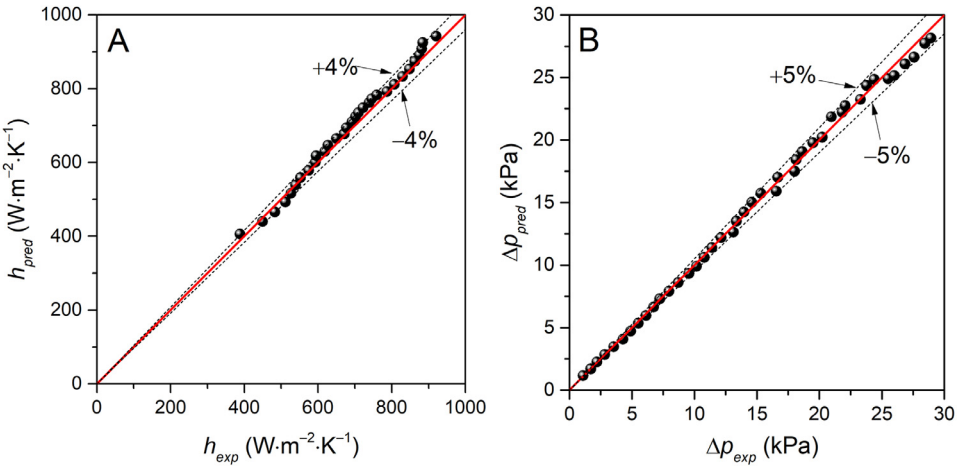

Fig. 3. Experimental and predicted values of **(A)** average convective heat transfer coefficient (h) and **(B)** pressure drop (Δp) for pristine [C_2C_1im][SCN]. Predicted values were calculated from the Sieder-Tate equation (Eq. (6)) and the Darcy-Weisbach formula (Eq. (10)), respectively. Solid line – diagonal; dashed lines – deviation boundaries. The data are shown numerically in Table S6 in Supplementary Material.

where k is the thermal conductivity of [C_2C_1im][SCN] at T (Table S3 in Supplementary Material), η and η_w are the dynamic viscosity values of [C_2C_1im][SCN] at T and T_w, respectively (the viscosity was reported in Table S7 and Fig. S3 in Supplementary Material of ref. [32]), and *Re*, *Pr* are the numbers of Reynolds (Eq. (8)) and Prandtl (Eq. (9)), respectively [48,54,55].

$$Re = \frac{vd\rho}{\eta} \tag{8}$$

$$Pr = \frac{C_p\eta}{k} \tag{9}$$

where v is the average velocity of [C_2C_1im][SCN] in measuring tube (0.01–0.7 m·s^{-1}), ρ is the density of [C_2C_1im][SCN] at T (Table S2 in Supplementary Material), and C_p is the specific isobaric heat capacity of [C_2C_1im][SCN] at T (Table S1 in Supplementary Material).

Similarly, the experimental pressure drop during the flow of pristine [C_2C_1im][SCN] was compared with the values calculated from the Darcy-Weisbach equation for fully-developed laminar flow in a cylindrical tube [48]:

$$\Delta p = \frac{64}{Re}\frac{L}{d}\frac{v^2}{2}\rho. \tag{10}$$

Fig. 3 illustrates the comparison of the experimental data on average convective heat transfer coefficient (Fig. 3A) and pressure drop (Fig. 3B) for [C_2C_1im][SCN] with the values obtained from Sieder-Tate equation (Eq. (6)) and Darcy-Weisbach formula (Eq. (10)), respectively. As can be seen, there is a reasonable agreement between experiment and theory. The observed deviations are about ±4% and ±5% for h and Δp, respectively. Moreover, these values fall within the range of determined measurement uncertainties of ±6% and ±11%, respectively (see Table S5 in Supplementary Material).

3. Results and discussion

The main stage of the research involved the analysis of positive and negative effects in the heat transfer of [C_2C_1im][SCN]-based INFs with MWCNT concentrations of 0.100 wt%, 0.175 wt%, and 0.250 wt%. This was accomplished through the experimental determination of average convective heat transfer coefficient h (Eq. (3)) and pressure drop Δp (Eq. (5)) in the laminar flow regime ($2 \le Re \le 100$, $100 \le Pr \le 150$, $200 \le Pe \le 10000$), respectively. This measuring range was a direct result of the syringe pump ability (pumping power). The experimental values of h and Δp were presented as a function of thermal Peclet number *Pe* (Eq. (11)), characterizing both physicochemical and hydrodynamic properties of the fluid. Peclet number is the product of Reynolds number (Eq. (8)), which defines the flow regime, and Prandtl number (Eq. (9)), which describes the relationship between momentum and thermal diffusivities [48,54,55].

$$Pe = \frac{vd\rho C_p}{k} \tag{11}$$

where k is the thermal conductivity of INFs at T (Table S3 in Supplementary Material and Table S4 in Supplementary Material of our previous work [32]). The relative combined standard uncertainty of *Pe* was estimated based on the method presented by Moffat [51] and equal to ±6% (see Part III of the Supplementary Material). All the obtained values of h, Δp, and *Pe* are collected in Tables S7 and S8 in Supplementary Material and shown in Figs. 4A and 5A.

Based on the average convective heat transfer coefficient h, the dimensionless average Nusselt number *Nu* was calculated [47,48]:

$$Nu = \frac{hd}{k}. \tag{12}$$

The obtained *Nu* values are collected in Table S7 in Supplementary Material and shown in Figs. 4B. The relative combined standard uncertainty of *Nu* is equal to ±8% (see Part III of the Supplementary Material).

Furthermore, the measured pressure drop Δp was used to calculate the Darcy friction factor f according to the equation [56–58]:

$$f = \frac{2d\Delta p}{L\rho v^2}. \tag{13}$$

The obtained results of f are collected in Table S8 in Supplementary Material and shown in Figs. 5B. The relative combined standard uncertainty of f is equal to ±12% (see Part III of the Supplementary Material).

As can be seen in Fig. 4A, the average convective heat transfer coefficient of INFs is much higher than that of the base IL, and it increases with increasing Peclet number as well as nanoparticle concentration. The maximum value of h is 1363 W·m^{-2}·K^{-1} for the most concentrated nanodispersion of 0.250 wt% at the highest Peclet number of ca. 10000. This is an increase of 48.1% compared to pristine IL under the same hydrodynamic conditions. In a similar literature study, Naddaf et al. [50] reported a maximum

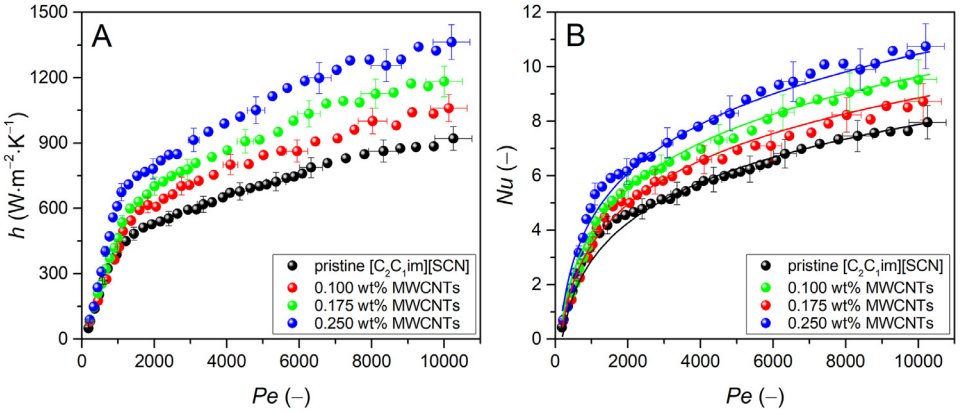

Fig. 4. "Positive effects" in heat transfer of analyzed INFs as a function of Peclet number (*Pe*): **(A)** experimental values of average convective heat transfer coefficient (*h*); **(B)** experimental data (points) and correlated values (lines, Eq. (14)) of average Nusselt number (*Nu*). The data are shown numerically in Table S7 in Supplementary Material.

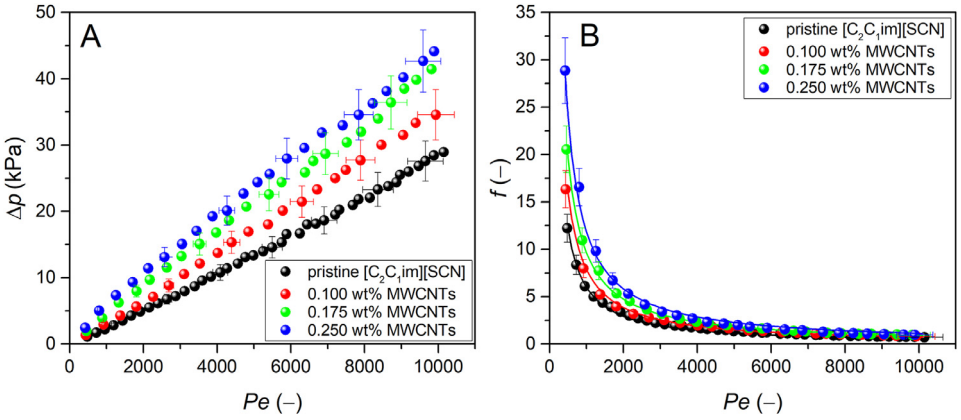

Fig. 5. "Negative effects" in heat transfer of analyzed INFs as a function of Peclet number (*Pe*): **(A)** experimental values of pressure drop (Δp); **(B)** experimental data (points) and correlated values (lines, Eq. (15)) of Darcy friction factor (*f*) – for *Pe* up to 3000, the point size is of order of error bar of *Pe*. The data are shown numerically in Table S8 in Supplementary Material.

11% increase in convective heat transfer coefficient (up to 380 $W \cdot m^{-2} \cdot K^{-1}$) during laminar flow ($50 < Re < 100$) of viscous diesel oil-based NFs containing 0.2 wt% GNPs or MWCNTs (with an average aspect ratio of 300) in a horizontal cylindrical tube. Also, Razi et al. [59] observed only a 5% enhancement of heat transfer coefficient (up to 230 $W \cdot m^{-2} \cdot K^{-1}$) in the range of $10 < Re < 100$ when testing CuO–base oil NF (0.2 wt% loading) under analogous hydrodynamic and geometric conditions. For comparison, in the case of more conventional Al_2O_3-distilled water nanodispersions, the maximum augmentation of laminar convective heat transfer coefficient in a straight cylindrical tube at low nanoparticle concentration (0.2 vol%) was approx. 25% (up to 950 $W \cdot m^{-2} \cdot K^{-1}$) in the range of $2500 < Pe < 6000$ [54].

Such remarkable enhancement of the average convective heat transfer coefficient of INFs obtained in this work cannot be explained simply by an increase in thermal conductivity, since the addition of 0.25 wt% in-house 7h MWCNTs to the base IL causes ca. 10% rise of this parameter (see Table S3 in Supplementary Material). It seems that the enhanced heat transfer of INFs may be related to the increased temperature gradient at the wall of measuring tube, caused by the non-uniform distribution of nanoparticles, especially with a high aspect ratio [54,60]. This phenomenon can be due to Brownian motion, stochastic movements, dispersion effects, nanoclustering, thermophoresis, and non-uniform shear rate across the tube [47,54]. Some researchers indicate that a key factor in the intensification of nanofluid heat transfer is a reduced thickness of thermal boundary layer [47,60]. The measured values of Prandtl number between 100 and 150 indicate that the thermal boundary layer is much thinner compared to the velocity boundary layer, thus the momentum diffusivity dominates over the thermal diffusivity. Moreover, at high nanofluid flow rates (high values of Reynolds and Peclet numbers), the nanoparticle fluctuations can flatten the temperature profile, which becomes similar to that seen in turbulent flow, and which increases the heat transfer [55].

The average convective heat transfer coefficient *h* is often presented in the form of dimensionless Nusselt number *Nu*, defined by Eq. (12). The obtained results for analyzed INFs clearly indicate that heat transfer by convection prevails over conduction and this effect significantly increases with Peclet number (Fig. 4B). The observed range of average Nusselt number $0 < Nu < 11$ is typical of nanofluid laminar flow [54,55,61–66] and much lower than in the case of turbulent motion, where *Nu* usually ranges from 50 to 250 [67–70].

The main purpose of preparing INFs is to enhance the heat transfer of base IL, however, it has a negative effect on the flow properties, because solid nanoparticles increase the viscosity and required pump power [71]. As can be seen in Fig. 5A, pressure drop Δp during the flow of INFs significantly increases with the loading of in-house 7h MWCNTs and Peclet number. For instance, the augmentation of Δp for the most concentrated INF at maximum *Pe* is 55.2% compared to the data for pristine $[C_2C_1im][SCN]$. This may be the result of aggregation and entanglement of long MWCNTs in IL [72]. No drag reduction is observed, although it was suggested in several previous research works on the rheology of low-concentrated MWCNT-based INFs [72–74]. The pressure drop measured by us is higher than in the case of other literature stud-

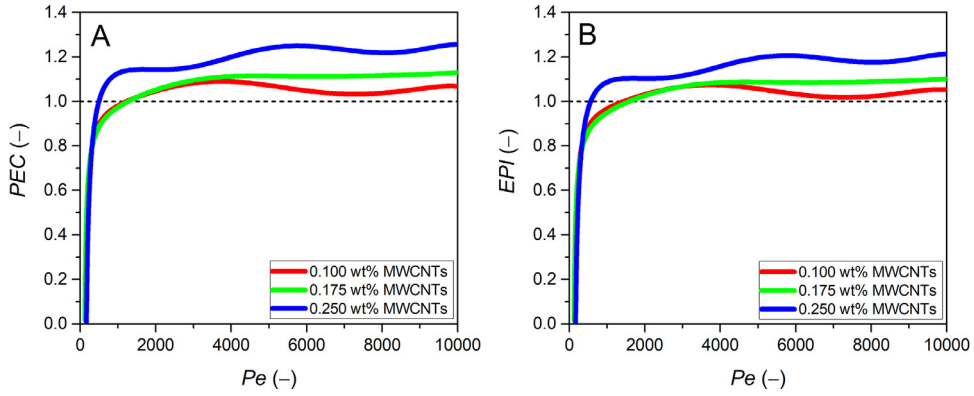

Fig. 6. Figures of merit of analyzed INFs for heat transfer purposes as a function of Peclet number (*Pe*): **(A)** performance evaluation criterion (*PEC*) and **(B)** efficiency-price index (*EPI*). Dashed lines – pristine [C_2C_1im][SCN]. The data are shown numerically in Table S9 in Supplementary Material.

ies, e.g., Razi et al. [59], observed a pressure loss up to 20 kPa at $Re = 100$, while testing the laminar flow of CuO–base oil nanofluid (2 wt% loading) in a horizontal cylindrical tube. Most likely, in-house 7h MWCNTs have a strong affinity to imidazolium cations providing more ordered structures, hence, the flow resistance of INFs is higher [75,76].

In hydraulics and fluid mechanics, the resistance in pipe flow is often presented in the form of Darcy friction factor *f*, defined by Eq. (13). As can be seen in Fig. 5B, the highest *f* occurs at the lowest values of Peclet number and significantly increases with the concentration of MWCNTs. This is associated with the growing importance of viscous forces in relation to inertial forces acting on the fluid. As a result, by increasing fluid velocity, the Darcy friction factor decreases. Our outcomes for 0.1 wt% INF show very good agreement with the data provided by Wang et al. [63] for nanodispersion containing distilled water and 0.05 vol% (i.e. about 0.1 wt%) carboxyl-functionalized MWCNTs with an average aspect ratio of 700. In our work and the above-mentioned literature study [63], in comparable flow range (i.e. $3500 < Pe < 10000$ and $30 < Re < 100$), the Darcy friction factor is equal to 2.2–0.8 and 2.1–0.8, respectively.

In the engineering practice of designing any heat transfer equipment, it is often necessary to use mathematical correlations between average Nusselt number *Nu* or Darcy friction factor *f* and their independent variables. Therefore, such useful empirical models for tested INFs have been proposed, respectively:

$$Nu = 0.9718 \cdot \log(Pe)^{1.827}(1+\phi)^{144.3} - 4.347 \tag{14}$$

$$f = 7038(Pe)^{-1.024}(1+\phi)^{513.5}. \tag{15}$$

The Eqs. (14) and (15) have two dimensionless independent variables: Peclet number *Pe* and volume fraction of nanoparticles ϕ. Their forms were determined via nonlinear regression analysis using the Nonlinear Surface Fit Tool with the Levenberg-Marquardt algorithm, available in OriginPro software (OriginLab, USA). The proposed Eqs. (14) and (15) very well describe the experimental data on heat transfer of analyzed INFs in the range of $200 \le Pe \le 10000$ and $0 \le \phi \le 0.00133$ (Figs. 4B and 5B). The calculated coefficient of determination is close to unity and takes values of $R^2 = 0.986$ and $R^2 = 0.994$ for Eq. (14) and Eq. (15), respectively. Importantly, the inherent assumption of the proposed empirical models is forced convection during a single-phase fully-developed laminar flow of both Newtonian or non-Newtonian fluid in a straight horizontal cylindrical tube.

3.1. Figures of merit

To clarify the trade-off between heat transfer enhancement and pressure drop penalty due to the presence of MWCNTs within the base IL, the non-dimensional performance evaluation criterion *PEC* was determined according to Eq. (16) [77]. The detailed derivation of *PEC* can be found in ref. [78]. It expresses the relation between the average Nusselt number improvement and the Darcy friction factor increase at constant pumping power conditions.

$$PEC = \frac{\frac{Nu_{INF}}{Nu_{IL}}}{\left(\frac{f_{INF}}{f_{IL}}\right)^{\frac{1}{3}}} \tag{16}$$

where Nu_{IL}, Nu_{INF} are the average Nusselt numbers for IL and INF, respectively, and f_{IL}, f_{INF} are the Darcy friction factors for IL and INF, respectively. The obtained results are collected in Table S9 in Supplementary Material and shown in Fig. 6A.

In order to verify the cost-effectiveness of adding MWCNTs to base IL, we proposed a new thermo-economic criterion called efficiency-price index *EPI* defined as:

$$EPI = \frac{PEC}{\left(\frac{\$_{INF}}{\$_{IL}}\right)} \tag{17}$$

with

$$\$_{INF} = \$_{IL} + \$_{MWCNTs} + \$_{UT} \tag{18}$$

where $\$_{INF}$ is the total cost of INF preparation, $\$_{IL}$ is the price of base IL, $\$_{MWCNTs}$ is the total cost of nanotube synthesis, and $\$_{UT}$ is the cost of dispersing MWCNTs in base IL by ultrasound treatment. A summary of the costs is shown in Table 1, while a detailed list of costs can be found in Table S4 in Supplementary Material. The calculated values of *EPI* are collected in Table S9 in Supplementary Material and shown in Fig. 6B.

As illustrated in Fig. 6A, *PEC* is higher than unity virtually in the entire measuring range, except for the lowest applied flow rates, i.e., at $Pe < 1000$. Hence, it can be concluded that the positive effects of improved heat transfer of studied INFs exceed the negative effects of augmented friction losses. Furthermore, an increase in the MWCNT concentration enhances the overall thermal performance of INFs. The maximum observed *PEC* of 1.26 is significant compared to the literature data on heat transfer performance in deep laminar flow regime ($Re < 100$) for conventional nanodispersions containing carbon nanoparticles and high-viscosity base liquids, e.g., MWCNTs/GNPs and diesel oil [50] or MWCNTs and heat transfer oil [79], for which the average *PEC* was about 1.1. Moreover, our results are comparable to the simulation data of [C_4C_1im][NTf_2] + Al_2O_3, determined by El-Maghlany and

Table 1
Material and preparation costs of analyzed INFs.

ID	IL volume (mL)	MWCNT concentration (wt%)	MWCNT weight (g)	$\$_{IL}$ ($)	$\$_{MWCNTs}$ ($)	$\$_{UT}$ ($)
Sample 1	150	0.100	0.1674	174.36	2.54	0.01
Sample 2	150	0.175	0.2933	174.36	4.44	0.01
Sample 3	150	0.250	0.4192	174.36	6.35	0.01

Minea [36], at much higher nanoparticle concentration (1 vol%) and Reynolds number ($100 < Re < 2000$).

A significant disadvantage of *PEC* is the omission of material and preparation costs of INFs. Therefore, we proposed a new non-dimensional thermo-economic criterion called efficiency-price index *EPI*, defined by the Eq. (17). The calculated values of *EPI* as a function of Peclet number are shown in Fig. 6B. The course of *EPI* and *PEC* curves is very similar except for a slight reduction in the value of *EPI* which depends on the dose of MWCNTs. The maximum value of *EPI* is 1.21, which is only of 3.5% lower than *PEC* under the same measuring conditions. These results clearly indicate that the addition of in-house 7h MWCNTs to $[C_2C_1im][SCN]$ is economically justified, as the total costs of synthesis and dispersion of nanotubes are insignificant compared to the price of base ionic liquid.

4. Conclusions

Our work is the first fully experimental analysis of the heat transfer performance of INFs in the laminar flow regime ($2 \leq Re \leq 100$, $100 \leq Pr \leq 150$, $200 \leq Pe \leq 10000$), taking into account both gains and losses from the use of this type of media. A detailed analysis of the results shows that the average convective heat transfer coefficient h and the pressure drop Δp increase significantly with nanoparticle concentration and nanodispersion flow rate. In the case of the most concentrated INF (0.25 wt%) at the maximum Pecklet number (ca. 10000), the enhancement of h and Δp reaches 48.1% and 55.2% compared to base IL, respectively. To clarify the trade-off between heat transfer improvement and pressure drop penalty due to the presence of MWCNTs within the base IL, two figures of merit have been introduced: performance evaluation criterion (*PEC*) and efficiency-price index (*EPI*). Both *PEC* and *EPI* are higher than unity in the entire measuring range, except for the lowest applied flow rates of INFs ($Pe < 1000$). The maximum observed values of *PEC* and *EPI* are equal to 1.26 and 1.21, respectively. These values clearly indicate that the addition of in-house 7h MWCNTs to $[C_2C_1im][SCN]$ is justified from both thermophysical and economic points of view.

Our research shows that when the concentration of MWCNTs increases, the heat transfer efficiency of INFs also rises (see *PEC* and *EPI* parameters in Fig. 6), thus, it would be worthwhile to make measurements on dispersions containing higher doses of the nanoparticles (> 0.25 wt%). However, this requires the use of a new closed-circuit installation with a much more powerful non-pulsating delivery pump, due to the significantly enhanced viscosity of such media. It would also be valuable to take measurements in the turbulent regime, since the drag reduction effect may occur and be beneficial to the overall heat transfer performance of INFs. Furthermore, an interesting possibility might be to study the heat transfer efficiency of nanodispersions based on other low-viscosity and low-toxicity ionic liquids, e.g., 1-ethyl-3-methylimidazolium dicyanamide $[C_2C_1im][DCA]$ or 1-ethyl-3-methylimidazolium tricyanomethanide $[C_2C_1im][TCM]$.

Declaration of Competing Interest

There are no conflicts to declare.

CRediT authorship contribution statement

Bertrand Jóźwiak: Conceptualization, Methodology, Validation, Formal analysis, Investigation, Data curtion, Visualization, Writing – original draft, Writing – review & editing. **Grzegorz Dzido:** Conceptualization, Methodology, Validation, Investigation, Resources, Writing – original draft, Supervision. **Anna Kolanowska:** Investigation, Resources. **Rafał G. Jędrysiak:** Investigation, Resources. **Edward Zorębski:** Investigation, Methodology, Validation, Formal analysis, Data curtion. **Heather F. Greer:** Investigation, Methodology, Resources. **Marzena Dzida:** Conceptualization, Methodology, Validation, Investigation, Resources, Writing – original draft, Writing – original draft, Writing – review & editing, Supervision, Project administration, Funding acquisition. **Sławomir Boncel:** Conceptualization, Methodology, Validation, Investigation, Resources, Writing – original draft, Writing – original draft, Visualization, Writing – review & editing, Supervision, Project administration, Funding acquisition.

Acknowledgments

BJ, GD, AK, RJ, EZ, MD, and SB thank the National Science Centre (Poland) for the financial support in the framework of OPUS Grant No. 2017/27/B/ST4/02748. HFG thanks the EPSRC Underpinning Multi-User Equipment Call (EP/P030467/1) for funding the TEM.

Supplementary materials

Supplementary material associated with this article can be found, in the online version, at doi:10.1016/j.ijheatmasstransfer.2021.121161.

References

[1] H. Esen, M. Inalli, M. Esen, Technoeconomic appraisal of a ground source heat pump system for a heating season in eastern Turkey, Energy Convers. Manag. 47 (2006) 1281–1297, doi:10.1016/j.enconman.2005.06.024.
[2] H. Esen, M. Inalli, M. Esen, A techno-economic comparison of ground-coupled and air-coupled heat pump system for space cooling, Build. Environ. 42 (2007) 1955–1965, doi:10.1016/j.buildenv.2006.04.007.
[3] M. Esen, T. Yuksel, Experimental evaluation of using various renewable energy sources for heating a greenhouse, Energy Build 65 (2013) 340–351, doi:10.1016/j.enbuild.2013.06.018.
[4] K. Singh, R. Das, Exergy optimization of cooling tower for HGSHP and HVAC applications, Energy Convers. Manag. 136 (2017) 418–430, doi:10.1016/j.enconman.2017.01.024.
[5] K. Singh, R. Das, Simultaneous optimization of performance parameters and energy consumption in induced draft cooling towers, Chem. Eng. Res. Des. 123 (2017) 1–13, doi:10.1016/j.cherd.2017.04.031.
[6] K. Singh, R. Das, An improved constrained inverse optimization method for mechanical draft cooling towers, Appl. Therm. Eng. 114 (2017) 573–582, doi:10.1016/j.applthermaleng.2016.12.002.
[7] K. Singh, R. Das, Improved Quantification of Exergy Destruction in Mechanical Cooling Tower Considering All Tower Inlet Parameters, J. Heat Transf. (2018) 140, doi:10.1115/1.4038479.
[8] L. Das, K. Habib, R. Saidur, N. Aslfattahi, S.M. Yahya, F. Rubbi, Improved Thermophysical Properties and Energy Efficiency of Aqueous Ionic Liquid/MXene Nanofluid in a Hybrid PV/T Solar System, Nanomaterials. 10 (2020) 1372, doi:10.3390/nano10071372.
[9] H.G. Zavaragh, A. Kaleli, F. Afshari, A. Amini, Optimization of heat transfer and efficiency of engine via air bubble injection inside engine cooling system, Appl. Therm. Eng. 123 (2017) 390–402, doi:10.1016/j.applthermaleng.2017.04.164.

[10] E. Ettefaghi, A. Rashidi, H. Ahmadi, S.S. Mohtasebi, M. Pourkhalil, Thermal and rheological properties of oil-based nanofluids from different carbon nanostructures, Int. Commun. Heat Mass Transf. 48 (2013) 178–182, doi:10.1016/j.icheatmasstransfer.2013.08.004.

[11] A.A. Balandin, Thermal properties of graphene and nanostructured carbon materials, Nat. Mater. 10 (2011) 569–581, doi:10.1038/nmat3064.

[12] C. Shen, G. Lv, S. Wei, C. Zhang, C. Ruan, Investigating the performance of a novel solar lighting/heating system using spectrum-sensitive nanofluids, Appl. Energy. 270 (2020) 115208, doi:10.1016/j.apenergy.2020.115208.

[13] F.E.B. Bioucas, S.I.C. Vieira, M.J.V. Lourenço, F.J.V. Santos, C.A. Nieto de Castro, Performance of heat transfer fluids with nanographene in a pilot solar collector, Sol. Energy. 172 (2018) 171–176, doi:10.1016/j.solener.2018.05.040.

[14] A. Alashkar, M. Gadalla, Thermo-economic analysis of an integrated solar power generation system using nanofluids, Appl. Energy. 191 (2017) 469–491, doi:10.1016/j.apenergy.2017.01.084.

[15] C.A. Nieto de Castro, S.M.S. Murshed, M.J.V. Lourenço, F.J.V. Santos, M.L.M. Lopes, J.M.P. França, Ionanofluids: New Heat Transfer Fluids for Green Processes Development, in: M.A. Inamuddin (Ed.), Green Solvents I, Springer, Dordrecht, the Netherlands, 2012, pp. 233–249, doi:10.1007/978-94-007-1712-1_8.

[16] A.P.C. Ribeiro, S.I.C. Vieira, J.M. França, C.S. Queirós, E. Langa, M.J.V. Lourenço, S.M.S. Murshed, C.A. Nieto de Castro, Thermal Properties of Ionic Liquids and Ionanofluids, in: A. Kokorin (Ed.), Ion. Liq. Theory Prop. New Approaches, InTech, Rijeka, Croatia, 2011, pp. 37–60, doi:10.5772/603.

[17] C.A. Nieto de Castro, A.P.C. Ribeiro, I.C. Salome, J.M.P. Franca, M.J.V. Lourenço, F.V. Santos, S.M.S. Murshed, P. Goodrich, C. Hardacre, Synthesis, Properties and Physical Applications of IoNanofluids, in: J. Kadokawa (Ed.), Ion. Liq. - New Asp. Future, InTech, Rijeka, Croatia, 2013, doi:10.5772/52596.

[18] W. Chen, C. Zou, X. Li, An investigation into the thermophysical and optical properties of SiC/ionic liquid nanofluid for direct absorption solar collector, Sol. Energy Mater. Sol. Cells. 163 (2017) 157–163, doi:10.1016/j.solmat.2017.01.029.

[19] A. Hosseinghorbani, M. Mozaffarian, G. Pazuki, Application of graphene oxide IoNanofluid as a superior heat transfer fluid in concentrated solar power plants, Int. Commun. Heat Mass Transf. 111 (2020) 104450, doi:10.1016/j.icheatmasstransfer.2019.104450.

[20] B. Bakthavatchalam, K. Habib, R. Saidur, B.B. Saha, K. Irshad, Comprehensive study on nanofluid and ionanofluid for heat transfer enhancement: A review on current and future perspective, J. Mol. Liq. 305 (2020) 112787, doi:10.1016/j.molliq.2020.112787.

[21] S.S. Prasad, R.D. Selvakumar, Heat transfer performance of Al_2O_3 – ($[C_4mim][NTf_2]$) nano-suspension in a 2−D channel for application in a flat plate solar collector, IOP Conf. Ser. Mater. Sci. Eng. 577 (2019) 012006, doi:10.1088/1757-899X/577/1/012006.

[22] T.C. Paul, A.K.M.M. Morshed, E.B. Fox, J.A. Khan, Thermal performance of Al_2O_3 Nanoparticle Enhanced Ionic Liquids (NEILs) for Concentrated Solar Power (CSP) applications, Int. J. Heat Mass Transf. 85 (2015) 585–594, doi:10.1016/j.ijheatmasstransfer.2015.01.071.

[23] S.I. Vieira, M.J.V. Lourenço, J.M. Alves, C.A.N. de Castro, Using Ionic Liquids and MWCNT's (Ionanofluids) in Pigment Development, J. Nanofluids. 1 (2012) 148–154, doi:10.1166/jon.2012.1017.

[24] P. Bose, D. Deb, S. Bhattacharya, Ionic liquid based nanofluid electrolytes with higher lithium salt concentration for high-efficiency, safer, lithium metal batteries, J. Power Sources. 406 (2018) 176–184, doi:10.1016/j.jpowsour.2018.10.050.

[25] M.-D. Avilés, N. Saurín, J. Sanes, F.-J. Carrión, M.-D. Bermúdez, Ionanocarbon Lubricants, The Combination of Ionic Liquids and Carbon Nanophases in Tribology, Lubricants. 5 (2017) 14, doi:10.3390/lubricants5020014.

[26] X. Shi, W. Huang, X. Wang, Ionic liquids–based magnetic nanofluids as lubricants, Lubr. Sci. 30 (2018) 73–82, doi:10.1002/ls.1405.

[27] K. Oster, C. Hardacre, J. Jacquemin, A.P.C. Ribeiro, A. Elsinawi, Understanding the heat capacity enhancement in ionic liquid-based nanofluids (ionanofluids), J. Mol. Liq. 253 (2018) 326–339, doi:10.1016/j.molliq.2018.01.025.

[28] J.M.P. França, M.J.V. Lourenço, S.M.S. Murshed, A.A.H. Pádua, C.A. Nieto de Castro, Thermal Conductivity of Ionic Liquids and IoNanofluids and Their Feasibility as Heat Transfer Fluids, Ind. Eng. Chem. Res. 57 (2018) 6516–6529, doi:10.1021/acs.iecr.7b04770.

[29] V.S. Patil, A. Cera-Manjarres, D. Salavera, C.V. Rode, K.R. Patil, A. Coronas, Influence of Silver Nanoparticles Morphologies on Density, Viscosity and Thermal Conductivity of Silver Nanofluids and Silver IoNanofluids, J. Nanofluids. 7 (2018) 246–257, doi:10.1166/jon.2018.1451.

[30] K. Oster, C. Hardacre, J. Jacquemin, A.P.C. Ribeiro, A. Elsinawi, Ionic liquid-based nanofluids (ionanofluids) for thermal applications: an experimental thermophysical characterization, Pure Appl. Chem. 91 (2019) 1309–1340, doi:10.1515/pac-2018-1114.

[31] A. Kazakov, J.W. Magee, R.D. Chirico, E. Paulechka, V. Diky, C.D. Muzny, K. Kroenlein, M. Frenkel, NIST Standard Reference Database 147: Ionic Liquids Database – ILThermo v2.0, National Institute of Standards and Technology, Gaithersburg, USA, 2017.

[32] B. Jóźwiak, G. Dzido, E. Zorębski, A. Kolanowska, R. Jędrysiak, J. Dziadosz, M. Libera, S. Boncel, M. Dzida, Remarkable Thermal Conductivity Enhancement in Carbon-Based Ionanofluids: Effect of Nanoparticle Morphology, ACS Appl. Mater. Interfaces. 12 (2020) 38113–38123, doi:10.1021/acsami.0c09752.

[33] T.C. Paul, AKM.M. Morshed, J.A. Khan, Nanoparticle Enhanced Ionic Liquids (NEILS) as Working Fluid for the Next Generation Solar Collector, Procedia Eng. 56 (2013) 631–636, doi:10.1016/j.proeng.2013.03.170.

[34] T.C. Paul, A.K.M.M. Morshed, E.B. Fox, J.A. Khan, Experimental investigation of natural convection heat transfer of Al_2O_3 Nanoparticle Enhanced Ionic Liquids (NEILs), Int. J. Heat Mass Transf. 83 (2015) 753–761, doi:10.1016/j.ijheatmasstransfer.2014.12.067.

[35] A.A. Minea, S.M.S. Murshed, A review on development of ionic liquid based nanofluids and their heat transfer behavior, Renew. Sustain. Energy Rev. 91 (2018) 584–599, doi:10.1016/j.rser.2018.04.021.

[36] W.M. El-Maghlany, A.A. Minea, Novel empirical correlation for ionanofluid PEC inside tube subjected to heat flux with application to solar energy, J. Therm. Anal. Calorim. 135 (2019) 1161–1170, doi:10.1007/s10973-018-7461-y.

[37] M. Ansarpour, E. Danesh, M. Mofarahi, Investigation the effect of various factors in a convective heat transfer performance by ionic liquid, ethylene glycol, and water as the base fluids for Al_2O_3 nanofluid in a horizontal tube: A numerical study, Int. Commun. Heat Mass Transf. 113 (2020) 104556, doi:10.1016/j.icheatmasstransfer.2020.104556.

[38] T.C. Paul, R. Mahamud, J.A. Khan, Multiphase modeling approach for ionic liquids (ILs) based nanofluids: Improving the performance of heat transfer fluids (HTFs), Appl. Therm. Eng. 149 (2019) 165–172, doi:10.1016/j.applthermaleng.2018.12.039.

[39] F.-F. Zhang, F.-F. Zheng, X.-H. Wu, Y.-L. Yin, G. Chen, Variations of thermophysical properties and heat transfer performance of nanoparticle-enhanced ionic liquids, R. Soc. Open Sci. 6 (2019) 182040, doi:10.1098/rsos.182040.

[40] E.I. Cherecheş, K.V. Sharma, A.A. Minea, A numerical approach in describing ionanofluids behavior in laminar and turbulent flow, Contin. Mech. Thermodyn. 30 (2018) 657–666, doi:10.1007/s00161-018-0634-x.

[41] E.I. Cherecheş, A.A. Minea, K.V. Sharma, A complex evaluation of $[C_2mim][CH_3SO_3]$– alumina nanoparticle enhanced ionic liquids internal laminar flow, Int. J. Heat Mass Transf. 154 (2020) 119674, doi:10.1016/j.ijheatmasstransfer.2020.119674.

[42] A. Alirezaie, M.H. Hajmohammad, A. Alipour, M. Salari, Do nanofluids affect the future of heat transfer? A benchmark study on the efficiency of nanofluids, Energy. 157 (2018) 979–989, doi:10.1016/j.energy.2018.05.060.

[43] A. Alirezaie, M.H. Hajmohammad, M.R.H. Ahangar, M.H. Esfe, Price-performance evaluation of thermal conductivity enhancement of nanofluids with different particle sizes, Appl. Therm. Eng. 128 (2018) 373–380, doi:10.1016/j.applthermaleng.2017.08.143.

[44] A.J.F. Mendonça, C.A. Nieto de Castro, M. Assael, W.A. Wakeham, The Economic Advantages of Accurate Transport Property Data for Heat Transfer Equipment Design, Rev. Port. Quím. 23 (1981) 7–11.

[45] J.M.P. França, C.A. Nieto de Castro, M.M. Lopes, V.M.B. Nunes, Influence of Thermophysical Properties of Ionic Liquids in Chemical Process Design, J. Chem. Eng. Data. 54 (2009) 2569–2575, doi:10.1021/je900107t.

[46] A. Kolanowska, A. Kuziel, Y. Li, S. Jurczyk, S. Boncel, Rieche formylation of carbon nanotubes – one-step and versatile functionalization route, RSC Adv. 7 (2017) 51374–51381, doi:10.1039/C7RA10525H.

[47] M.M. Heyhat, F. Kowsary, A.M. Rashidi, M.H. Momenpour, A. Amrollahi, Experimental investigation of laminar convective heat transfer and pressure drop of water-based Al_2O_3 nanofluids in fully developed flow regime, Exp. Therm. Fluid Sci. 44 (2013) 483–489, doi:10.1016/j.expthermflusci.2012.08.009.

[48] F. Kreith, R.M. Manglik, M.S. Bohn, Principles of heat transfer, Cengage Learning, 7th ed., Stamford, USA, 2011.

[49] M.I. Stewart, Heat Transfer Theory, in: M.I. Stewart (Ed.), Surf. Prod. Oper., 3rd ed., Gulf Professional Publishing, Boston, MA, USA, 2014, pp. 39–97, doi:10.1016/B978-0-12-382207-9.00003-2.

[50] A. Naddaf, S. Zeinali Heris, B. Pouladi, An experimental study on heat transfer performance and pressure drop of nanofluids using graphene and multi-walled carbon nanotubes based on diesel oil, Powder Technol. 352 (2019) 369–380, doi:10.1016/j.powtec.2019.04.078.

[51] R.J. Moffat, Describing the uncertainties in experimental results, Exp. Therm. Fluid Sci. 1 (1988) 3–17, doi:10.1016/0894-1777(88)90043-X.

[52] E.N. Sieder, G.E. Tate, Heat Transfer and Pressure Drop of Liquids in Tubes, Ind. Eng. Chem. 28 (1936) 1429–1435, doi:10.1021/ie50324a027.

[53] I. Tosun, Evaluation of Transfer Coefficients: Engineering Correlations, in: I. Tosun (Ed.), Model. Transp. Phenom., 2nd ed., Elsevier, Amsterdam, 2007, pp. 59–115, doi:10.1016/B978-044453021-9/50005-1.

[54] S.Z. Heris, M.N. Esfahany, S.Gh. Etemad, Experimental investigation of convective heat transfer of Al2O3/water nanofluid in circular tube, Int. J. Heat Fluid Flow. 28 (2007) 203–210, doi:10.1016/j.ijheatfluidflow.2006.05.001.

[55] M.T.H. Mosavian, S.Z. Heris, S.G. Etemad, M.N. Esfahany, Heat transfer enhancement by application of nano-powder, J. Nanoparticle Res. 12 (2010) 2611–2619, doi:10.1007/s11051-009-9840-6.

[56] S.R. Chaurasia, R.M. Sarviya, Thermal performance analysis of CuO/water nanofluid flow in a pipe with single and double strip helical screw tape, Appl. Therm. Eng. 166 (2020) 114631, doi:10.1016/j.applthermaleng.2019.114631.

[57] X. Peng, D. Wang, G. Wang, Y. Yang, S. Xiang, Investigation of heat transfer performance and flow characteristic in helically coiled-twisted flat tube, Exp. Heat Transf. 33 (2020) 419–439, doi:10.1080/08916152.2019.1656300.

[58] W. He, R. Mashayekhi, D. Toghraie, O.A. Akbari, Z. Li, I. Tlili, Hydrothermal performance of nanofluid flow in a sinusoidal double layer microchannel in order to geometric optimization, Int. Commun. Heat Mass Transf. 117 (2020) 104700, doi:10.1016/j.icheatmasstransfer.2020.104700.

[59] P. Razi, M.A. Akhavan-Behabadi, M. Saeedinia, Pressure drop and thermal characteristics of CuO–base oil nanofluid laminar flow in flattened tubes under constant heat flux, Int. Commun. Heat Mass Transf. 38 (2011) 964–971, doi:10.1016/j.icheatmasstransfer.2011.04.010.

[60] S.K. Das, S.U.S. Choi, H.E. Patel, Heat Transfer in Nanofluids—A Review, Heat Transf. Eng. 27 (2006) 3–19, doi:10.1080/01457630600904593.

[61] Y. Yang, Z.G. Zhang, E.A. Grulke, W.B. Anderson, G. Wu, Heat transfer properties of nanoparticle-in-fluid dispersions (nanofluids) in laminar flow, Int. J. Heat Mass Transf. 48 (2005) 1107–1116, doi:10.1016/j.ijheatmasstransfer.2004.09.038.
[62] D. Ashtiani, M.A. Akhavan-Behabadi, M.F. Pakdaman, An experimental investigation on heat transfer characteristics of multi-walled CNT-heat transfer oil nanofluid flow inside flattened tubes under uniform wall temperature condition, Int. Commun. Heat Mass Transf. 39 (2012) 1404–1409, doi:10.1016/j.icheatmasstransfer.2012.07.017.
[63] J. Wang, J. Zhu, X. Zhang, Y. Chen, Heat transfer and pressure drop of nanofluids containing carbon nanotubes in laminar flows, Exp. Therm. Fluid Sci. 44 (2013) 716–721, doi:10.1016/j.expthermflusci.2012.09.013.
[64] C. Selvam, S. Harish, D.M. Lal, Effective thermal conductivity and rheological characteristics of ethylene glycol-based nanofluids with single-walled carbon nanohorn inclusions, Fuller. Nanotub. Carbon Nanostructures. 25 (2017) 86–93, doi:10.1080/1536383X.2016.1261285.
[65] A. Tahiri, K. Mansouri, Theoretical investigation of laminar flow convective heat transfer in a circular duct for a non-Newtonian nanofluid, Appl. Therm. Eng. 112 (2017) 1027–1039, doi:10.1016/j.applthermaleng.2016.10.137.
[66] H.-H. Ting, S.-S. Hou, Investigation of Laminar Convective Heat Transfer for Al2O3-Water Nanofluids Flowing through a Square Cross-Section Duct with a Constant Heat Flux, Materials. 8 (2015) 5321–5335, doi:10.3390/ma8085246.
[67] A.A. Hachicha, Z. Said, S.M.A. Rahman, E. Al-Sarairah, On the thermal and thermodynamic analysis of parabolic trough collector technology using industrial-grade MWCNT based nanofluid, Renew. Energy. 161 (2020) 1303–1317, doi:10.1016/j.renene.2020.07.096.
[68] B. Saleh, L.S. Sundar, Entropy generation and exergy efficiency analysis of ethylene glycol-water based nanodiamond + Fe3O4 hybrid nanofluids in a circular tube, Powder Technol. 380 (2021) 430–442, doi:10.1016/j.powtec.2020.12.006.
[69] S. Zhang, L. Lu, T. Wen, C. Dong, Turbulent heat transfer and flow analysis of hybrid Al2O3-CuO/water nanofluid: An experiment and CFD simulation study, Appl. Therm. Eng. 188 (2021) 116589, doi:10.1016/j.applthermaleng.2021.116589.
[70] L.S. Sundar, M.K. Singh, A.C.M. Sousa, Turbulent heat transfer and friction factor of nanodiamond-nickel hybrid nanofluids flow in a tube: An experimental study, Int. J. Heat Mass Transf. 117 (2018) 223–234, doi:10.1016/j.ijheatmasstransfer.2017.09.109.
[71] B. Jóźwiak, S. Boncel, Rheology of ionanofluids – A review, J. Mol. Liq. 302 (2020) 112568, doi:10.1016/j.molliq.2020.112568.
[72] B. Wang, X. Wang, W. Lou, J. Hao, Rheological and Tribological Properties of Ionic Liquid-Based Nanofluids Containing Functionalized Multi-Walled Carbon Nanotubes, J. Phys. Chem. C. 114 (2010) 8749–8754, doi:10.1021/jp1005346.
[73] C.Y. Neo, J. Ouyang, Functionalized carbon nanotube-induced viscosity reduction of an ionic liquid and performance improvement of dye-sensitized solar cells, Electrochimica Acta. 85 (2012) 1–8, doi:10.1016/j.electacta.2012.08.041.
[74] A.G.M. Ferreira, P.N. Simões, A.F. Ferreira, M.A. Fonseca, M.S.A. Oliveira, A.S.M. Trino, Transport and thermal properties of quaternary phosphonium ionic liquids and IoNanofluids, J. Chem. Thermodyn. 64 (2013) 80–92, doi:10.1016/j.jct.2013.04.013.
[75] R. Pamies, C. Espejo, F.J. Carrión, A. Morina, A. Neville, M.D. Bermúdez, Rheological behavior of multiwalled carbon nanotube-imidazolium tosylate ionic liquid dispersions, J. Rheol. 61 (2017) 279–289, doi:10.1122/1.4975108.
[76] R. Pamies, M.D. Avilés, J. Arias-Pardilla, F.J. Carrión, J. Sanes, M.D. Bermúdez, Rheological study of new dispersions of carbon nanotubes in the ionic liquid 1-ethyl-3-methylimidazolium dicyanamide, J. Mol. Liq. 278 (2019) 368–375, doi:10.1016/j.molliq.2019.01.074.
[77] M. Zarringhalam, A. Karimipour, D. Toghraie, Experimental study of the effect of solid volume fraction and Reynolds number on heat transfer coefficient and pressure drop of CuO–Water nanofluid, Exp. Therm. Fluid Sci. 76 (2016) 342–351, doi:10.1016/j.expthermflusci.2016.03.026.
[78] R.L. Webb, N.-H. Kim, Principles of Enhanced Heat Transfer, 2nd ed., CRC Press, Boca Raton, FL, USA, 2005.
[79] M.M. Derakhshan, M.A. Akhavan-Behabadi, S.G. Mohseni, Experiments on mixed convection heat transfer and performance evaluation of MWCNT–Oil nanofluid flow in horizontal and vertical microfin tubes, Exp. Therm. Fluid Sci. 61 (2015) 241–248, doi:10.1016/j.expthermflusci.2014.11.005.